Mechanics & Industry **20**, 615 (2019)
© AFM, EDP Sciences 2019
https://doi.org/10.1051/meca/2019054

Mechanics & Industry

Available online at:
www.mechanics-industry.org

REGULAR ARTICLE

Investigation on the skidding dynamic response of rolling bearing with local defect under elastohydrodynamic lubrication

Jianxiong Kang[1,2], Yanjun Lu[1,2,*], Yongfang Zhang[3], Cheng Liu[4], Sha Li[5], and Norbert Müller[6]

[1] School of Mechanical and Precision Instrument Engineering, Xi'an University of Technology, Xi'an 710048, PR China
[2] State Key Laboratory of Digital Manufacturing Equipment and Technology, Huazhong University of Science and Technology, Wuhan 430074, PR China
[3] School of Printing, Packaging Engineering and Digital Media Technology, Xi'an University of Technology, Xi'an 710048, PR China
[4] Key Laboratory of Manufacturing Equipment of Shaanxi Province, Xi'an University of Technology, Xi'an 710048, PR China
[5] Key Laboratory of NC Machine Tools & Integrated Manufacturing Equipment of the Ministry of Education, Xi'an University of Technology, Xi'an 710048, PR China
[6] College of Engineering, Michigan State University, East Lansing, MI 48824, USA

Received: 2 July 2018 / Accepted: 17 June 2019

Abstract. The rolling element skidding may lead to the failure of the rolling bearing. The skidding characteristics can be effectively analyzed by using dynamic response of the rolling bearing. A dynamic model is established to investigate the vibration response of the rolling bearing with local defect on inner/outer race in this paper. In the proposed model, the rolling element skidding, contact stiffness and displacement, the interaction force between ball and race, the interaction force between cage and race, elastohydrodynamic lubrication are taken into consideration. The dynamic responses of the rolling bearing with the rolling element skidding are solved by the proposed model in the time and frequency domains. The effects of defect size, rotational speed, external load, and compound factors on skidding characteristics are investigated. The proposed model is verified by the experiments. The results show that the rolling element skidding leads to the significant difference of dynamic characteristics in the time and frequency domains, which aggravates the failure of the rolling bearings.

Keywords: Dynamic response / rolling bearing / local defect / skidding / elastohydrodynamic lubrication

1 Introduction

The rolling bearing is one of the most important parts of the rotating machinery and widely used in automotive industry, aviation, spaceflight, navigation and other rotational machinery. It is a complex component of a machine and makes up of outer race, inner race, rolling element, cage, housing, oil film. The local defects (the crack, pitting and peeling, etc.) may generate when the rolling bearing operates for a long-time. When the local defects occur, the bearing will rotate unsteadily. In order to diagnose the bearing operation condition immediately, the condition monitoring and fault diagnosis are adopted in the field of bearing. The dynamics analysis method is an effective method for analyzing the bearing operation condition. The dynamics model can reflect the actual dynamic response characteristics with the time-varying. It is necessary to further research of the rolling bearing dynamics, which is important to explore the vibration mechanism of the rolling bearings.

The vibration response has been widely used to diagnose the rolling bearing defects. When the rolling bearing has local defects on the rolling element and the inner/outer race, the vibration response will change significantly. Jone [1] firstly put forward the quasi-static model of the rolling bearing. The slipping friction and motion were investigated based on the race control hypothesis. Gupta [2] established a three-dimensional dynamic model of the rolling bearings. In Gupta's model, the centrifugal force, gyroscopic, lubrication and the cage effects are all take into consideration. However, the localized defects are not considered in the Gupta's model. Due to the important role of dynamic response in the fault diagnosis of the rolling bearings, most scholars have established dynamic models to investigate the response

* e-mail: yanjunlu@xaut.edu.cn

characteristics of the rolling bearings. Garad et al. [3] predicted the presence of the defects on the outer and inner races based on 2-DOF (degree of freedom) model. The effect of defects on vibration behaviors of the rolling bearing was investigated by the 2-DOF model. Niu et al. [4] proposed a dynamic model to investigate vibration responses of the angular contact ball bearings with ball defects, the three dimensional motion of ball was considered based on Gupta's model. The result shows that the geometrical characteristics and operation conditions affect the frequency property of envelope spectrum, it also increases the difficulty of diagnosing the ball defects. Wang et al. [5] presented a method to analyze the friction of the deep-groove ball bearings with varying circumference radial preload, the experiment was conducted to verify the validity of the proposed method under different operation conditions. Based on the 4-DOF mathematical model, Yu et al. [6] analyzed the vibration characteristics of the deep groove ball bearing by the Runge-Kutta method. Moshrefzadeh et al. [7] investigated the planetary gears vibration properties under the healthy and faulty conditions. A lumped parameter model (LPM) of planetary gear trains was integrated with a comprehensive bearing model. By the proposed model, the dynamic responses of the system were identified and analyzed. The defect frequencies of inner/outer race, ball/roller and their side bands were discussed thoroughly. Jamadar et al. [8] presented a new fault diagnosis approach of the deep groove ball bearing with localized surface defects on the races. The experimental results show that the proposed approach is effective for diagnosing the surface defects on the race of the deep groove ball bearing. The above scholars established the dynamic model to analyze the characteristics of the vibration response. However, most scholars did not consider the effect of elastohydrodynamic lubrication (EHL) between the bearing race and rolling element. Dewangan et al. [9] proposed a resistance method to measure the lubricant film thickness based on Hertz contact theory. The resistive lubricant film thickness was calculated based on elliptical and circular contact area of the two lubricants. The result showed that the resistance method can predict the failure of the rolling bearing, and it also can be used for online condition monitoring of the rolling element bearings. Bizarre et al. [10] established a 5-DOF nonlinear model by considering the effect of the EHL, the equivalent stiffness and damping parameters were evaluated under different loading conditions. The result showed that the model is feasible to analyze the complex rotating systems supported by oil lubricant. Yang et al. [11] presented a semi-analytical method to investigate the defect characteristic frequency of the ball bearing system with/without defect on the outer race. The nonlinear characteristics of a rotor-ball bearing system were analyzed using their presented method. Wang et al. [12] presented an improved nonlinear dynamic model with consideration of the preload condition, surface waviness, Hertz contact and EHL. Servais et al. [13] proposed a new efficient method to compute the transverse loads without the race control hypothesis, and obtained a relationship between the ball bearing kinematics and transverse loads. The skidding of the rolling element is neglected in the above works. However, the skidding characteristics affect the dynamic responses of the rolling bearings. Xu et al. [14] proposed an analytical method to calculate the optimum preload at different speeds. The results showed that the method can effectively calculate the optimum preload under the condition of the skidding and rolling of the rolling bearing. Randall et al. [15] presented a combined dynamic model of the gears-bearings system, in which an extended fault in the inner/outer race of the rolling element bearings can be studied in the presence of gear interaction. Wang et al. [16] developed a dynamic model for angular contact ball bearing to investigate the contact characteristics and motion of ball-race conformity. The results revealed that the contact pressure and skidding between the ball and race have some influence on the ball-race conformity. Wang et al. [17] established the dynamic model to investigate the skidding of angular contact ball bearing with the interaction between race and ball. The skidding and EHL are considered in the proposed model, the results showed that the different conditions significantly affect the behavior of skidding. Han et al. [18] presented a three-dimensional nonlinear dynamic model to predict the skidding between the ball and race under different load conditions. Niu et al. [19] proposed a new method for accurately calculating the ball passing frequencies based on their dynamic model of the rolling bearing with localized defects. The relative skidding, cage effect, local defect and relative motion factors were introduced in their model. The proposed model was verified by the experiment. Liu et al. [20] established a new dynamic model to formulate the local surface defect of the cylindrical roller bearing. The relationship between the time-varying contact stiffness and the load-displacement of the rolling element and the race were investigated in the proposed model. The effects of the radial load, defect sizes, contact deformation and contact force between roller and race were investigated using the proposed model.

In this paper, a dynamics model is proposed to investigate the vibration response of the rolling bearing with the local defect. In order to simulate the operation condition of the rolling element, the rolling element skidding, interaction force between ball and race, cage/race interactions, damping and EHL are taken into consideration. Based on the proposed model, the dynamic responses of the rolling bearing with rolling element skidding are solved. The dynamic characteristics are investigated under different operation conditions. The proposed model is applied to diagnose and monitor the local defect on inner/outer race of the rolling bearing, and it is verified by the experiment results.

2 Dynamic model of rolling bearing

2.1 Model simplification

In order to investigate the dynamic responses of the rolling bearing, the dynamic model of the rolling bearing is established based on the Hertz contact theory. The contact behaviors between the rolling bearing and rolling element can be analyzed by using a equivalent spring-stiffness-damping model, as shown in Figure 1. In Figure 1, K is the

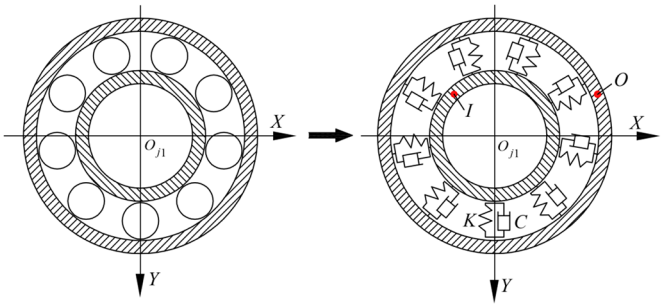

Fig. 1. Simplified model of the rolling bearing.

contact stiffness, C is the damping, I is the inner race, O is the outer race, O_{j1} is the shaft center of the rolling bearing.

According to the Hertz contact theory, the contact force is expressed as

$$F = K\delta^n, \tag{1}$$

where K is the contact stiffness of the rolling bearing, δ is the contact displacement between the rolling element and rolling bearing. For the rolling bearing, n is equal to 3/2.

The functions of the contact stiffness are written as

$$k_i = \frac{2\sqrt{2}\left(\dfrac{E}{1-\sigma^2}\right)}{3\left(\sum \rho_i\right)^{1/2}}\left(\frac{1}{\delta_i^*}\right)^{3/2} \tag{2}$$

$$k_o = \frac{2\sqrt{2}\left(\dfrac{E}{1-\sigma^2}\right)}{3\left(\sum \rho_o\right)^{1/2}}\left(\frac{1}{\delta_0^*}\right)^{3/2} \tag{3}$$

where E is the material elastic modulus of the rolling bearing, σ is the Poisson's ratio, $\sum\rho_i$ is the sum of the curvature of the inner race, $\sum\rho_o$ is the sum of the curvature of the outer race, δ_i^* is the dimensionless contact deformation of the inner race, δ_o^* is the dimensionless contact deformation of the outer race.

2.2 Calculation of contact deformation

The center of the rolling bearing varies with the load, and consequently changes the contact geometric relationship between the rolling element and rolling bearing, as shown in Figure 2. In Figure 2, O_{j2} is the center of the race after deformation. The contact deformation is described as follows

$$\delta' = x\sin\theta_i + y\cos\theta_i - c' \tag{4}$$

where x, y are the deflections of the inner race along X- and Y-axes, θ_i is the contact angle between the ith rolling element and rolling race, c' is the radial clearance of the rolling bearing.

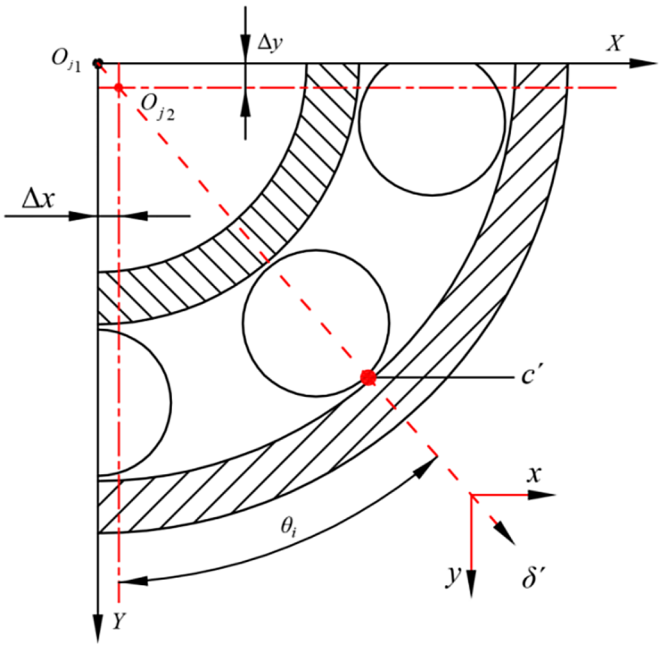

Fig. 2. Geometric relation of the contact deformation.

The expression of θ_i is written as

$$\theta_i = \frac{2\pi(i-1)}{z} + (\omega_c - \omega_s)t + \theta_0 \tag{5}$$

where z is the total number of the rolling element, i is the rolling element number, ω_s is the shaft velocity, θ_0 is the initial contact angle. ω_c is the cage velocity, and it is defined as

$$\omega_c = \left(1 - \frac{d}{D}\right)\frac{\omega_s}{2} \tag{6}$$

where d is the diameter of the rolling element, D is the pitch diameter.

2.3 Local defect model of inner/outer race

The local defect can be occurred on the inner/outer race of the rolling bearing after continuously working. When the rolling elements pass the race with local defect, the contact deformation changes significantly. In this paper, the crack defect is taken as an example to investigate the influence of the local defect on the dynamic response of the rolling bearing based on the built model. The profile of the local defect is simplified to the rectangle, as shown in Figure 3. In Figure 3, L is the length of the local defect.

The contact process of the rolling element is shown in Figure 4. In Figure 4, B is the width of the local defect, Φq is the defect angle, $H_{\max}$ is the maximum additional displacement.

When the rolling element passes through the local defect, the contact displacement between the rolling element and bearing race changes, and consequently leads to an additional displacement. The additional

displacement can be obtained by

$$H_f = \begin{cases} H_{\max}\sin\left[\dfrac{\pi}{\Phi_q}(\mathrm{mod}(\Phi_{di},2\pi)-\Phi_0)\right] & 0 \le \mathrm{mod}(\Phi_{di},2\pi)-\Phi_0 \le \Phi_q \\ 0 & \text{other} \end{cases} \tag{7}$$

where Φ_0 is the initial position angle of the ith rolling element to local defect, $H_{\max}$ is determined by the sizes of the rolling element and local defect, which is given by

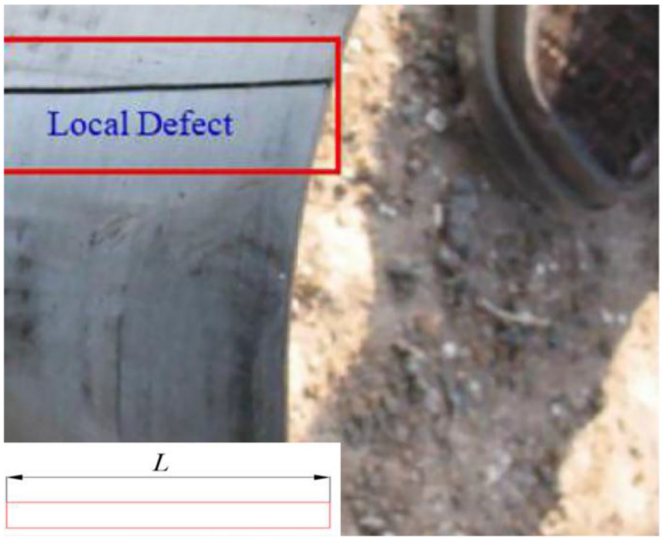

Fig. 3. Simplified model of the local defect.

$$H_{\max} = \frac{d}{2} - \sqrt{\left(\frac{d}{2}\right)^2 - (0.5B)^2}. \tag{8}$$

The expression of Φ_q is given by

$$\Phi_q = \arcsin\left(\frac{B}{r}\right) \tag{9}$$

where r is the radius of the inner/outer race. Φ_{di} is the angular position of the ith rolling element with respect to X-axis, and it can be expressed as

$$\Phi_{di} = \frac{2\pi}{z}(i-1) + \omega_c t. \tag{10}$$

The final contact displacement can be expressed by following equation

$$\delta = x\sin\theta_i + y\cos\theta_i - (c' + H_f). \tag{11}$$

2.4 Race/cage interactions

The interaction between the cage and guide race occurs with the action of the hydrodynamic pressure of the lubricant. Figure 5 shows the interaction force between cage and race (outer race). The interaction friction between the cage and guide race (outer race) can be expressed as

$$F_{cx} = -\frac{\eta_0 u_1 B^3}{c_1^2}\frac{\varepsilon^2}{(1-\varepsilon^2)^2}(\omega_i + \omega_c) \tag{12}$$

$$F_{cy} = \frac{\pi\eta_0 u_1 B_1^3}{4c_1^2}\frac{\pi\varepsilon}{(1-\varepsilon^2)^{3/2}}(\omega_i + \omega_c) \tag{13}$$

where η_0 is the viscosity of oil film, u_1 is the entrainment velocity of oil film, B_1 is the width of the centering surface of the cage, ε is the relative eccentricity of the cage center, c_1 is the size of the cage guide clearance. The expressions of u_1 and ε are given as follows

$$u_1 = R_1(\omega_i + \omega_c) \tag{14}$$

$$\varepsilon = \frac{e}{c_1} \tag{15}$$

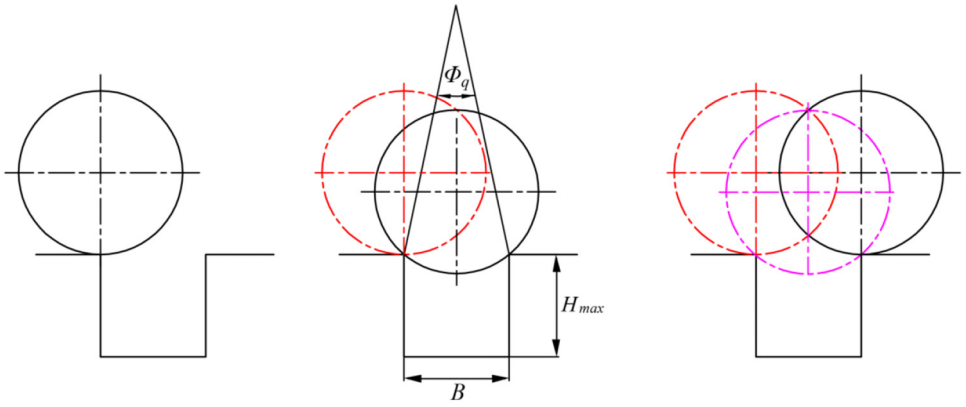

Fig. 4. Contact process of the rolling element.

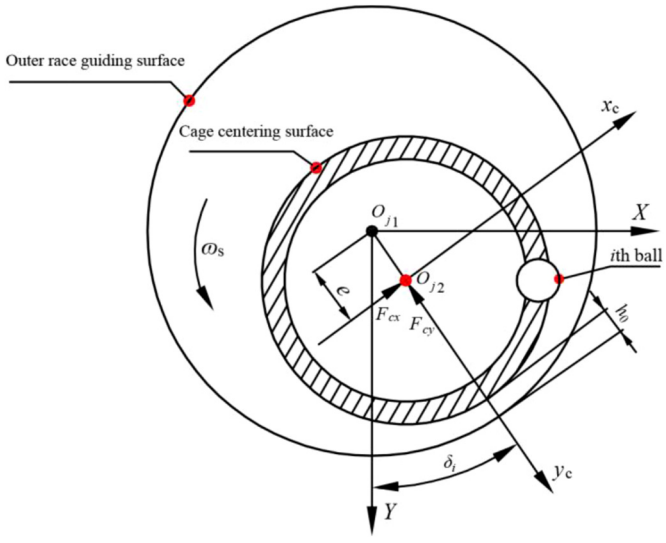

Fig. 5. Interaction force between cage and race (outer race).

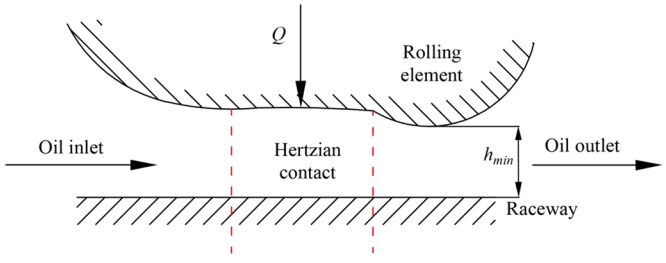

Fig. 6. Rolling element/race contact model EHL.

where R_1 is the radius of the centering surface of the cage, e is the relative variation of the cage center.

3 The calculation of point contact EHL

The parameters of the oil film changes with the temperature and pressure. In this paper, in order to simplify the calculation, the temperature and pressure are assumed to be constant. The contact model of the EHL between the rolling element and the race is shown in Figure 6.

3.1 Calculation the thickness and stiffness of the oil film

Based on the theoretical and experimental investigation, the Hamrock and Dowson [21] proposed a formula to calculate the minimum oil film thickness of the elliptical point contact. The minimum oil film thickness is written as

$$H' = \frac{3.63U'^{0.68}G^{0.49}(1-e^{-0.68k})}{Q'^{0.073}} \tag{16}$$

where U' is the dimensionless velocity parameter, G is the dimensionless material parameter, k is the ellipticity, Q' is the dimensionless load parameter, and it can be written as

$$Q' = \frac{Q}{E'R'^2} \tag{17}$$

where E' is the equivalent elastic modulus of material, R' is the equivalent radius of the rolling bearing in the rotational direction, Q is the external load. The expressions of E' and R' are written as

$$E' = \frac{E}{1-\sigma^2} \tag{18}$$

$$R' = \frac{d}{2}(1 \mp \gamma) \tag{19}$$

where '–' indicates the rolling element contact with the inner race, '+' indicates the rolling element contact with the outer race, the γ is calculated by $\gamma = (d\cos\alpha)/d_m$.

The central oil film thickness of contact area of the ellipse point contact is given as

$$H_O = \frac{2.69U'^{0.67}G^{0.53}(1-0.61e^{-0.73k})}{Q'^{0.067}}. \tag{20}$$

The minimum oil film thickness of the elliptical point contact can be expressed as

$$h_{\min} = H'R'. \tag{21}$$

According to the definition of stiffness, the oil film stiffness in the Hertz contact area can be expressed as

$$k_y = \frac{dQ}{dH_O}. \tag{22}$$

In the Hertz contact area, the damping of the oil film is little effect on the dynamic response. Thus, the oil film damping is neglected in the Hertz contact area in this part.

3.2 Calculation of the stiffness and damping of oil film in the inlet region

In the inlet region of the oil film, it is assumed that the sinusoidal vibration has happened near the contact point of the rolling element in the normal direction. The supporting load in the contact area can be expressed as [22]

$$Q_r = \frac{4\eta_0 u_x R' a}{h_{\min}^2\left(\frac{k_y}{k_o}+1\right)}\tau + j\frac{6.66\pi\eta_0 R'^{1.5}a}{\sqrt{2}h_{\min}^{1.5}}\omega\delta_t \tag{23}$$

where u_x is the entrainment velocity of the rolling element/race, a is the long semi-axis length of the contact ellipse, ω is the oscillating frequency.

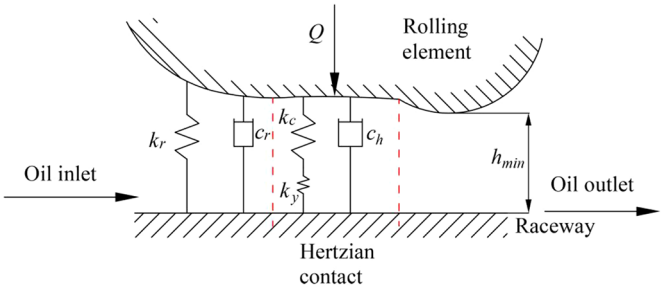

Fig. 7. Contact model of the stiffness and damping.

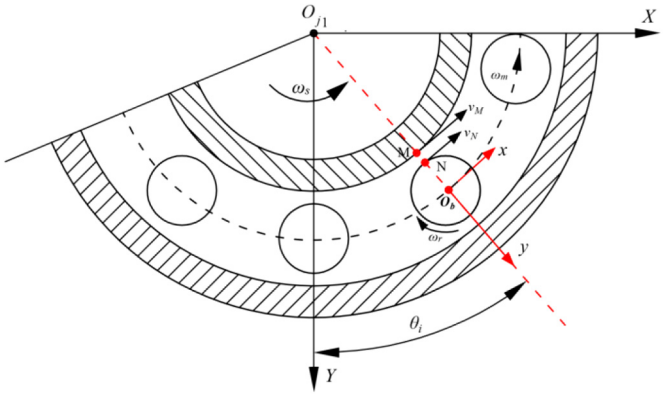

Fig. 8. Interaction between the race and rolling element.

The stiffness and damping of the oil film in the inlet region can be expressed as

$$k_r = \frac{4\eta_0 u_x R' a}{h_{\min}^2\left(\frac{k_y}{k_o}+1\right)} \tag{24}$$

$$c_r = \frac{6.66\pi\eta_0 u_x R'^{1.5} a}{\sqrt{2}h_{\min}^{1.5}}. \tag{25}$$

3.3 Calculation of total contact stiffness and damping

The relationship among the rolling element, bearing race and oil film is shown in Figure 7. According to the series-parallel model, the expressions functions of the stiffness and damping can be written as

$$k_{zi} = \frac{k_y k_i}{k_y + k_i} + k_r \tag{26}$$

$$k_{zo} = \frac{k_y k_o}{k_y + k_o} + k_r \tag{27}$$

$$K_z = \left[1/\left({}^{1}/_{k_{zi}}\right)^{1/n} + \left({}^{1}/_{k_{zo}}\right)^{1/n}\right]^n \tag{28}$$

$$C = c_h + c_r. \tag{29}$$

4 Skidding of the rolling element

The speed difference between the rolling element and race leads to the skidding of the rolling element due to the uneven load distribution. Figure 8 shows the interaction between the inner race and rolling element.

As shown in Figure 8, the linear velocity of the contact point M can be expressed as

$$v_M = \omega_s R_i \tag{30}$$

where R_i is the radius of the inner race.

The rolling element operates around the outer race center of the rolling bearing. It also operates around the center of itself. The linear velocity of the contact point N can be expressed as

$$v_N = \omega_m(R_i + \delta - h_{\min}) + \omega_r(R_r - \delta) \tag{31}$$

where ω_m is the angular velocity of the rolling element, ω_r is the rotation angular velocity of the rolling element.

The relative skidding speed between the point M and point N on the inner race can be given by

$$\Delta v = v_M - v_N. \tag{32}$$

Considering the EHL, the relative skidding speed can be obtained by

$$\Delta v_i' = \eta_0 \Delta v. \tag{33}$$

4.1 Calculation of oil film resistance

The frictional force of the oil film affects the friction of the rolling element directly. Hence, it is necessary to calculate the friction of the oil film. In this study, a typical traction curve of the EHL proposed by Gupta's [2] is used to calculate the friction of the oil film. The relationship between the friction coefficient and relative velocity is shown in Figure 9. As shown in Figure 9, the friction coefficient can be given by

$$\mu = \begin{cases} 0.04|\Delta v| & 0 < |\Delta v| < 0.05 \\ 0.02 & |\Delta v| \geq 0.05 \end{cases}. \tag{34}$$

Hence, the oil film resistance can be expressed as

$$F_i = -\mu N_i \frac{\Delta v'}{|\Delta v'|}. \tag{35}$$

5 Dynamic equation

According to the analysis of the local defect model under EHL, the the external force is balanced with the inertial

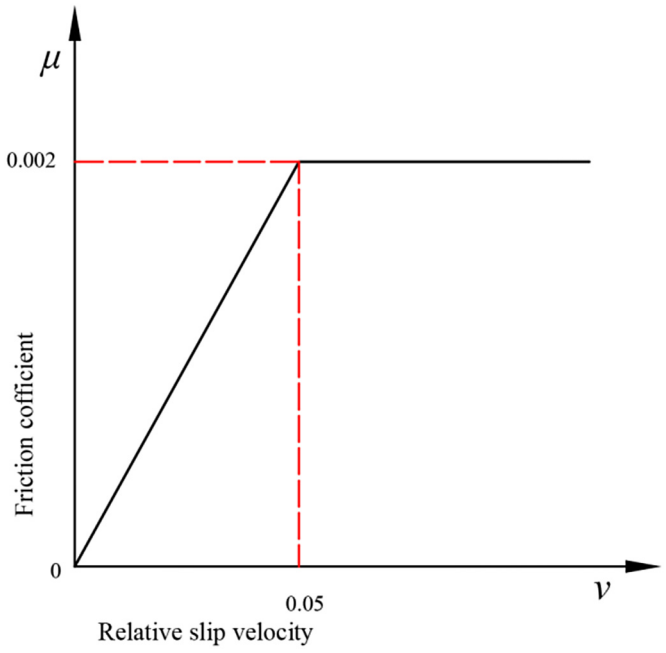

Fig. 9. Relation of the friction coefficient and relative velocity.

force, damping force, contact force caused by the elastic deformation and oil film force. The dynamic equations are written as

$$M\ddot{x}+C\dot{x}+\left(K_z\sum_{i=1}^{z}\beta\left[x\sin\theta_i+y\cos\theta_i-(c'+H_f)\right]^{\frac{3}{2}}+F_{cy}\right)\sin\theta_i +(F_i-F_{cx})\cos\theta_i=F_x \tag{36}$$

$$M\ddot{y}+C\dot{y}+\left(K_z\sum_{i=1}^{z}\beta\left[x\sin\theta_i+y\cos\theta_i-(c'+H_f)\right]^{\frac{3}{2}}+F_{cy}\right)\cos\theta_i +(F_i+F_{cx})\sin\theta_i=F_y \tag{37}$$

where M is the mass of inner race and shaft, C is the total damping coefficient, K_z is the total stiffness, β is the load parameter for the ith rolling element, and it can be expressed as

$$\beta=\begin{cases}1 & \delta>0\\ 0 & \delta\le 0\end{cases}. \tag{38}$$

6 Results and discussions

The SKF 6205 deep groove ball bearing with local defect is investigated, the outer race is fixed with the house, the inner race is fixed with the shaft. The bearing parameters are shown in Table 1. The influence of defect length and depth on dynamic response can be neglected in this paper because the crack defect size is merely little. The width and depth of the defect sizes are set as 0.1778 mm. In order to verify the proposed model, the test data of Case Western Reserve University is adopted for the model verification. The test rig consists of a 2 HP motors. The motor shaft supported by the test bearings. The faults are introduced into the test bearings with different fault diameters (the 7 mils, 14 mils, 21 mils). Vibration signal is collected using accelerometers, which are placed at the 12 o'clock position at both the drive end and fan end of the motor housing. Digital data is collected at 12 000 samples per second, and data is also collected at 48 000 samples per second for drive end bearing faults. Outer raceway faults are stationary faults, therefore placement of the fault relative to the load zone of the bearing has a direct impact on the vibration response of the motor/bearing system [23].

Table 1. Deep groove ball bearing parameters of SKF 6205.

Parameter	Value
Inner race diameter (D_i, mm)	25
Outer race diameter (D_o, mm)	52
Rolling element diameter (d, mm)	8.0
Number of rolling element (z)	9
Contact angle (θ, degree)	0
Radial clearance (c', μm)	20
Damping coefficient (c_h, N·s/m)	100

Table 2. Theoretical values of the rotational frequency, BPFI and BPFO.

Speed	f_s	f_i	f_o
1750 r/min	29.17	157.94	104.56

A fourth order Runge-Kutta method is used to calculate the equations (36) and (37). The rotational speed of the shaft is 1750 rpm. The fault characteristic frequency is a important signal to diagnose the rolling bearing, it also can recognize the position (inner race or out race) of the defect. The theoretical calculations of the Ball Pass Frequency Inner race (BPFI) and Ball Pass Frequency Outer race (BPFO) can be conducted by the following equations

$$f_i=\frac{zf_s}{2}\left(1+\frac{d}{d_m}\cos\theta\right) \tag{39}$$

$$f_o=\frac{zf_s}{2}\left(1-\frac{d}{d_m}\cos\theta\right) \tag{40}$$

where f_s is the rotational frequency.

The theory values of the characteristic frequency for shaft rotation, inner and outer race at the speed of 1750 rpm are shown in Table 2.

6.1 Reasonability of established model

In order to obtain the dynamic response of the proposed model, the dynamic equations are solved firstly. The radial load is 450 N, the time step used in the numerical investigation is 10^{-5} s, the initial displacements in X and Y direction are chosen to be 10^{-6} m.

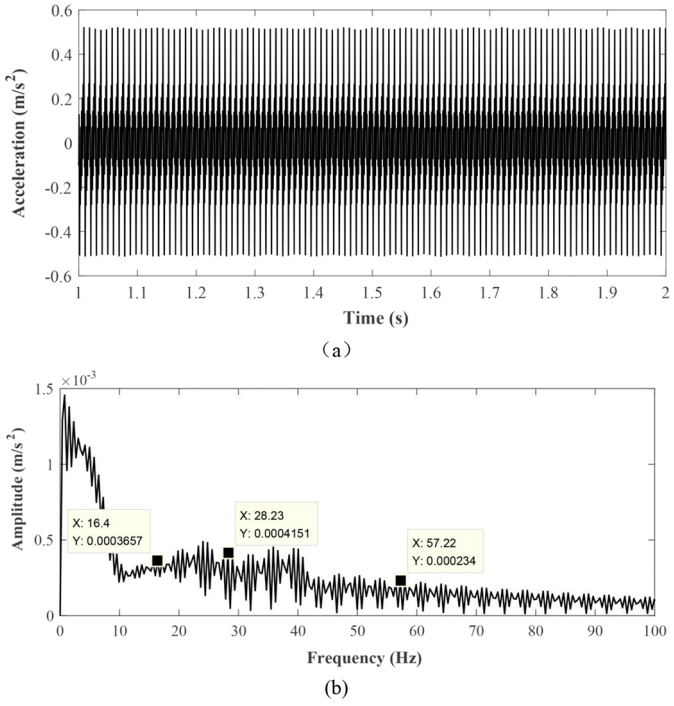

Fig. 10. Simulation signal of the healthy bearing.

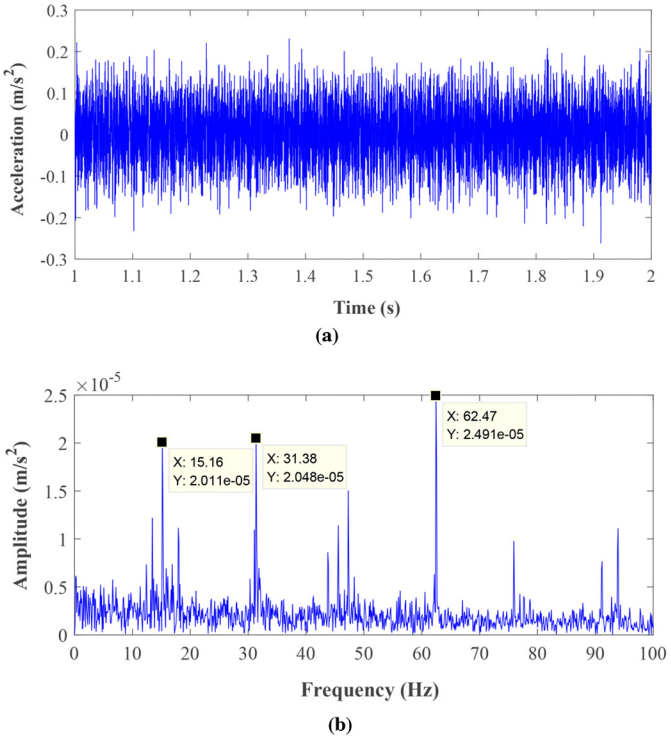

Fig. 11. Test signal of the healthy bearing.

By solving the equations (36) and (37), the dynamic responses of the acceleration with time-varying are acquired. Figure 10 is the simulated signal of the healthy bearing, Figure 10a plots the acceleration signal in the time domain, and Figure 10b gives the frequency domain signal which is obtained by the fast Fourier transform from Figure 10a. In Figure 10a, it can be seen that the response curve shows a stable periodic and no impulse signal. This means that the bearing is healthy at running time. As shown in Figure 10b, the unstable impulse signal is observed at the initial operation stage. With the continuing operation of the bearing, the amplitude of frequency signal tends to be stable, and then the rotational frequency (28.23 Hz) and doubling frequency (57.22 Hz) are appeared. The unstable signal in the frequency domain is caused by the start-up characteristics. Figure 11 shows the test signals of the healthy bearing in the time and frequency domains. From Figure 11a, it can be shown that there are some slight impacts during the operation of the bearing. The impact signal component is caused by the misalignment of the bearing and the environmental noise. By reducing the noise and envelope analysis of the original signals, the FFT method is used to obtain the spectrum. It can be concluded from the Figure 11a that the time-varying signal is the stable periodic signal approximately. The frequency domain signal of the healthy bearing is shown in Figure 11b. The rotational frequency and doubling frequency of the signal are 31.38 Hz and 62.47 Hz respectively. The test and simulation frequency are in good agreement by comparison of Figures 10b and 11b. Comparing the simulation with the test frequency, the error of the frequencies are very small. Therefore, the model is verified by the comparison.

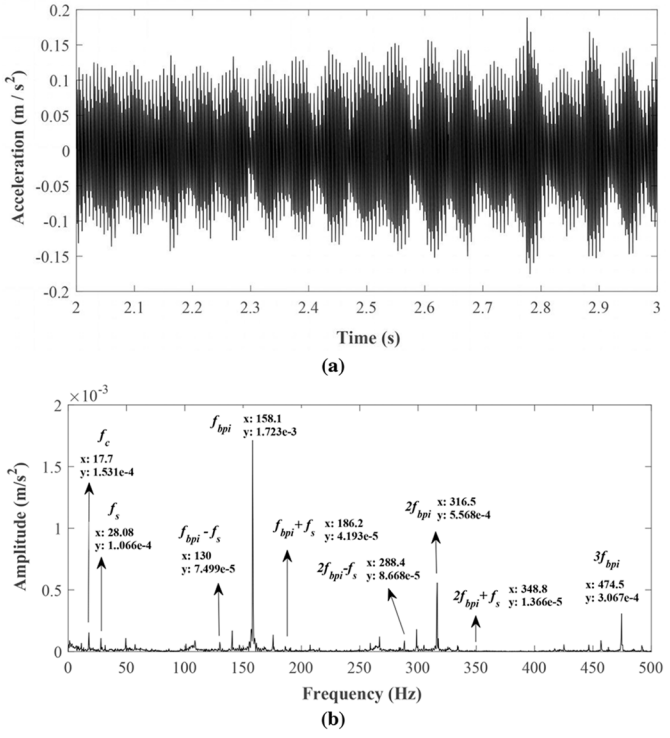

Fig. 12. Simulation signal of the inner race with local.

Figure 12 shows the signal of inner race with local defect in time and frequency domains. As shown in Figure 12a, the periodic pulses signal of the time domain is irregular. The FFT is applied to obtain the Figure 12b. The fault characteristic frequency and side band can be observed in

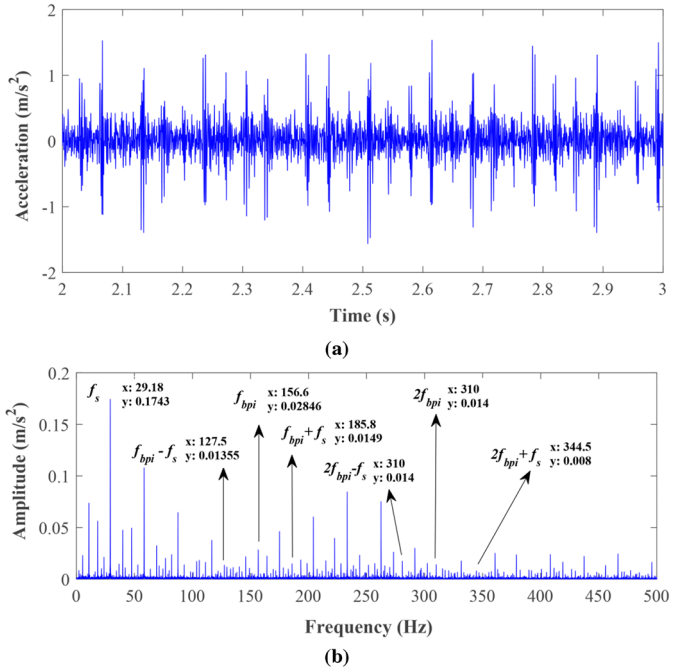

Fig. 13. Test signal of the inner race with local defect.

Figure 12b. The fault characteristic frequency is produced by the defect of the inner race, and the side-bands is caused by the modulation of the rotation frequency. Figures 13a and b are the test signals of the inner race with local defect in the time and frequency domains, the envelope analysis and noise reduction are used to process the test signal. The periodic impact signal is also observed in Figure 13a. Due to the external interference, the time domain signal in Figure 13a is less stable than Figure 12a. As shown in Figure 13b, the characteristic frequency of the test signal is 156.6 Hz. The BPFI of the simulation signal (158.1 Hz) and experiment (156.6 Hz) signal is close to the fault characteristic frequency. Therefore, the proposed model is validated by comparing the dynamic response signals with the experimental results. Figures 14 and 15 show the simulation and test signals of the outer race with local defect in time and frequency domains. By analyzing the results of the Figures 14a and 15a, the impulse signal and periodic features are also observed. The same method is also used to acquire the fault characteristic frequency of the outer race. As shown in Figures 14b and 15b, the numerical value of the BPFO are 104.4 Hz and 104.8 Hz respectively. The side band disappears because of the fixed outer race. The low numerical value error of the fault characteristic frequency proved that the model is verified.

6.2 Effect of defect size and external load on dynamic response

In this section, the effect of different operation conditions on the vibration response of the SKF 6205 deep groove ball bearing is investigated by the proposed model. The influence of local defect size on the dynamic response is also studied when the rotating speed is 1750 rpm and the external load is 450 N. Figures 16a and b are the spectrum

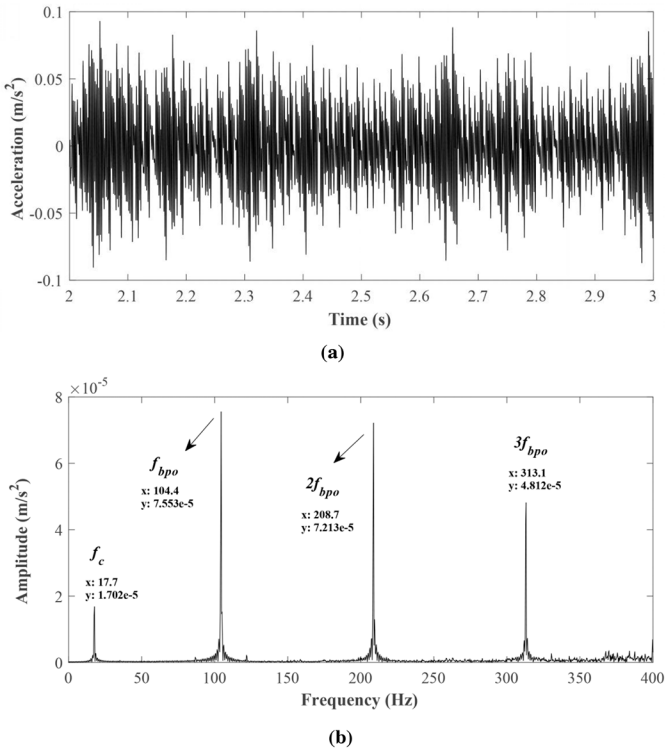

Fig. 14. Simulation signal of the outer race with local defect.

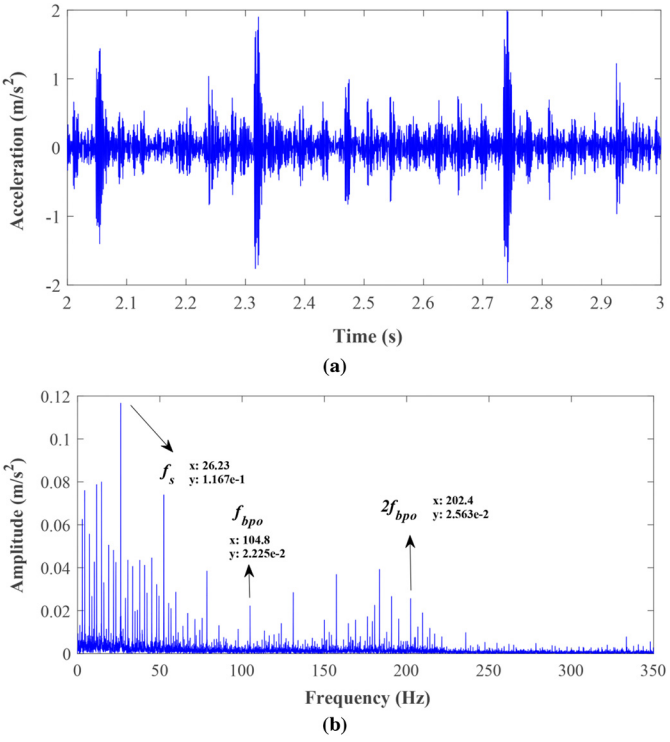

Fig. 15. Test signal of the outer race with local defect.

of inner and outer race with local defect size of 0.3556 mm. As shown in Figures 16a and b, the characteristic frequencies and double frequency have no change compared with Figures 12b and 14b. Figures 17a and b are the

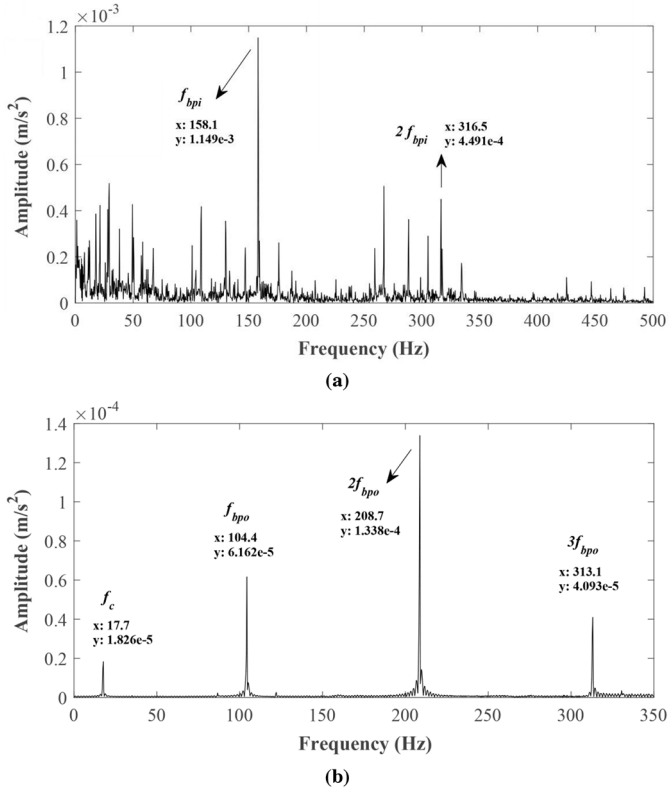

Fig. 16. Spectra of the inner and outer race with local defect size of 0.3556 mm.

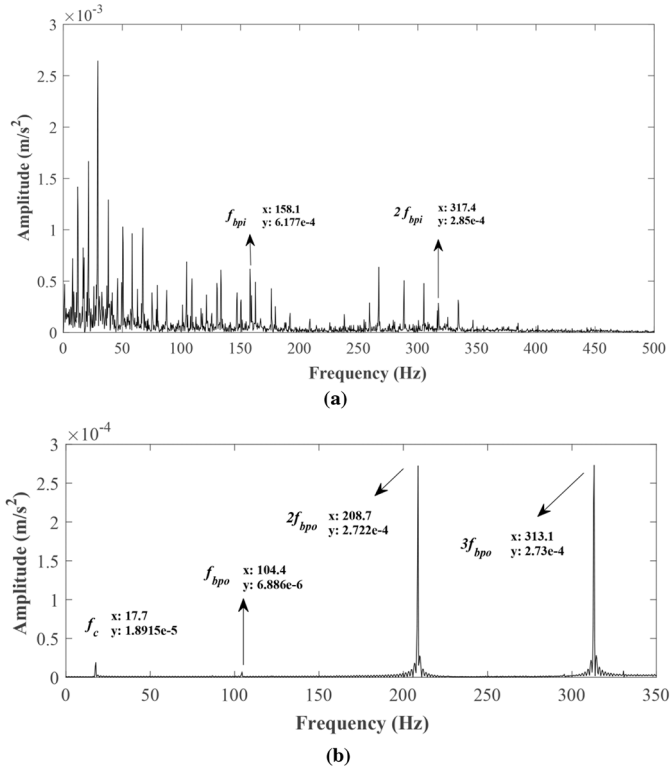

Fig. 17. Spectra of the inner and outer race with local defect size of 0.5334 mm.

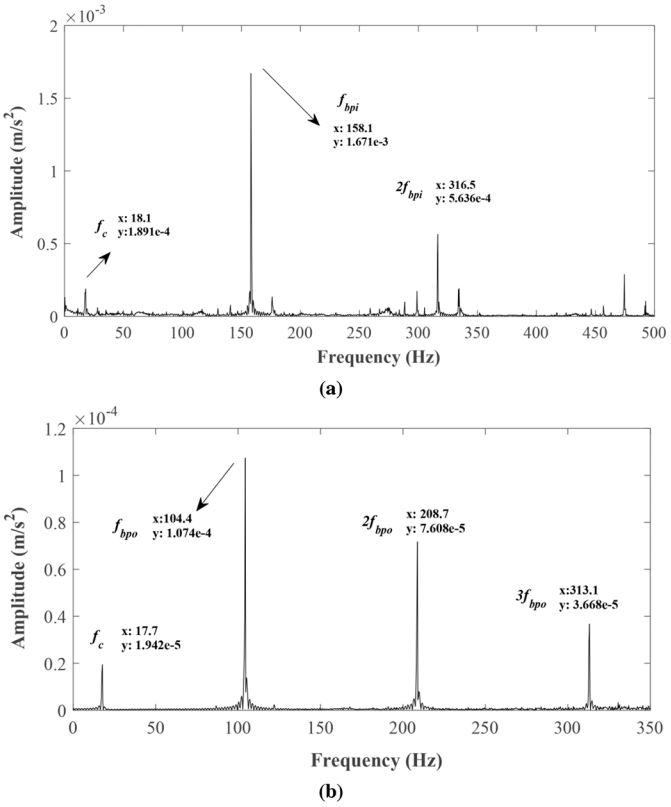

Fig. 18. Spectra of the inner and outer race with local defect under load 500 N.

spectrum of inner and outer race with local defect size of 0.5334 mm respectively. It can be see from Figures 17a and b that the characteristic frequencies are invariant. However, the amplitudes of the inner and outer race in Figures 17a and b changes with the defect sizes. By comparing the characteristic frequencies corresponding to the defect sizes 0.1778 mm, 0.3556 mm and 0.5334 mm, it can be observed that the amplitude of BPFO (Ball Pass Frequency Outer) increases with the increase of the defect size. However, the amplitude of BPFI (Ball Pass Frequency Inner) decreases with the increase of the defect size. The change of the amplitude is relatively large for the outer ring. The sideband of the frequency increases significantly for the inner ring. Therefore, the defect size has greater effect on the response amplitude of the outer race than the inner race.

The effects of external loads on dynamic response are investigated, as shown in Figures 18 and 19. In Figures 18 and 19, the rotational speed is 1750 rpm, and defect size is 0.1778 mm, and the external loads are 500 N and 800 N respectively. Comparing the Figure 12b, Figure 14b with Figure 18 and Figure 19, it can be observed that the frequency characteristics are invariable. A conclusion can be drawn that increasing the load is disadvantage to stabilize operation of the rolling bearing with the local defect. However, comparing the Figure 18a with Figure 19a, the amplitudes of the one-frequency decreases with the increase of external load, and the amplitude of double frequency is increases with the increase of the external load. It indicates that the occurrence of the skidding is low when the rolling element under the heavy

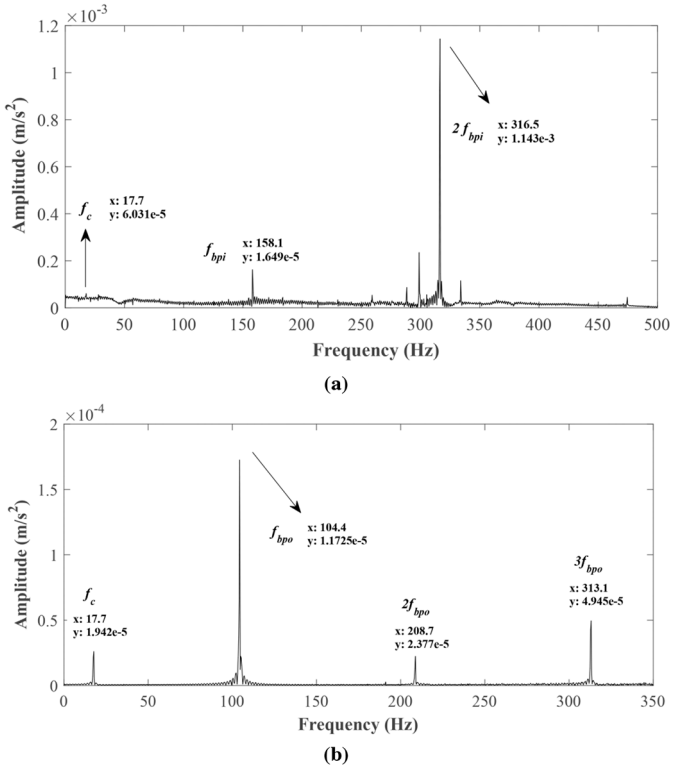

Fig. 19. Spectra of the inner and outer race with local defect under load 800 N.

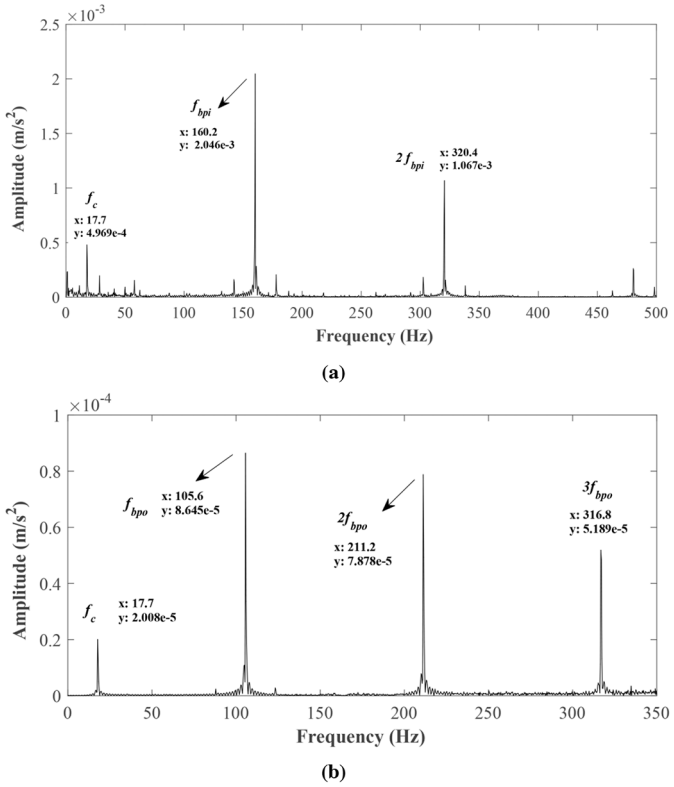

Fig. 20. Spectra of the inner and outer race with local defect at the speed of 1772 rpm.

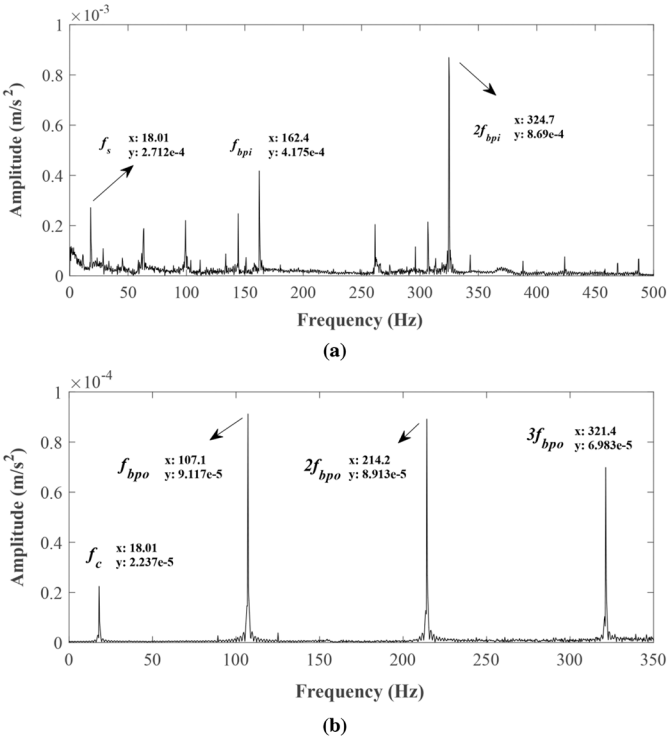

Fig. 21. Spectra of the inner and outer race with local defect at the speed of 1797 rpm.

load. As for the outer race, the first order frequency increases, the other characteristic frequencies relatively decrease. In particular, the increasing external load is disadvantage to the stable running of the deep groove ball bearing with local defect.

6.3 Effect of speed and compound factors on dynamic response

The characteristic frequencies are mainly controlled by the rotational speed. So the operational speed is an important factor for investigating the dynamic response of the rolling bearing. Figures 20 and 21 are the spectra of the inner and outer race with local defect. In Figures 20 and 21, the external load is 450 N, the defect size is 0.1778 mm, and the shaft rotational speeds are 1772 rpm and 1797 rpm respectively. Comparing the characteristic frequencies of Figures 20 and 21 with theoretical value, the results show that the relative error is very small. As shown in Figures 20 and 21, by discussing the effect of the rotational speed on dynamic response, it can be concluded that the rotational speed has a great influence on the vibration response of the deep groove ball bearing with the local defect. In order to improve the bearing life, it's necessary to control the rotational speed when the local defect occurs.

The dynamic response of the deep groove ball bearing under the combined factors (load and speed) is also studied, as shown in Figure 22. In Figure 22, the defect size is 0.1778 mm, the external load is 800 N, and the shaft rotational speed is 1797 rpm. The results in

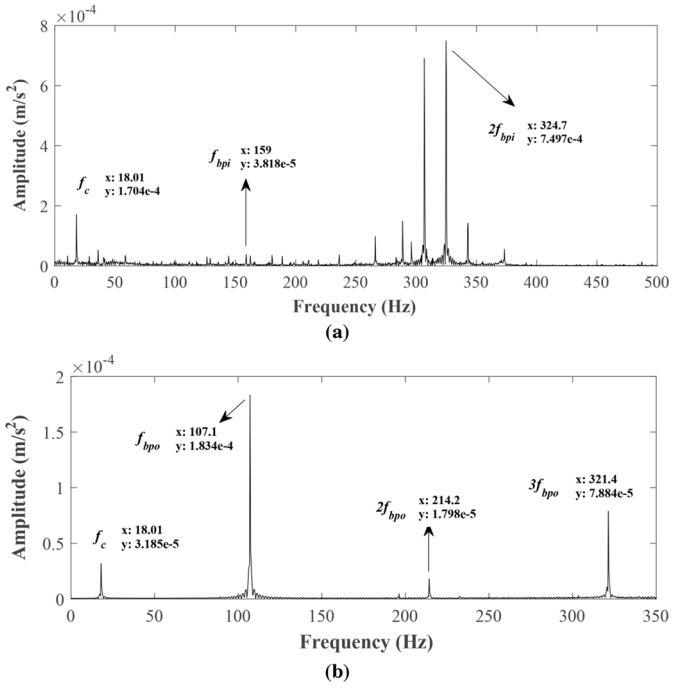

Fig. 22. Spectra of the inner and outer race with local defect under compound factors (external load is 800 N, shaft rotation is 1797 rpm).

Figures 21 and 22 show that the amplitudes of the inner race and out race vary greatly. It indicates that the occurrence of the skidding is relatively lower at lower rotational speed under the same external load.

7 Conclusion and prospect

A dynamic model is proposed to investigate the vibration response of the rolling element with local defect on inner/outer race in this paper. To achieve the velocity and acceleration, the dynamics equations are solved by the fourth order Runge-Kutta method. The effects of defect size, rotational speed, external load, and compound factors on skidding characteristics are investigated by the proposed model. The main conclusions are as follows:

– The proposed model is validated by comparing the dynamic response signals with the experimental results. The good consistency of the simulation and test signals verify that the proposed model can be used to investigate the dynamic response of the rolling bearing with the local defect.
– The increase of defect size and external load can lead to the change of the amplitude of spectrum, and aggravate the vibration of the rolling bearing and its operation stability. At the low-speed stage, the skidding with heavy load is smaller than light.
– The vibration response of the rolling bearings with the local defects is greatly affected by the change of velocity. At the same rotational speed, the external load has a great influence on skidding, and the effect of high speed and heavy load on skidding is less than that of high speed and light load.

The proposed model can be used to diagnose the fault of the rolling bearing in this paper. The evolution of the local defect of the rolling bearing is not considered. In the next research, we will devote ourselves to construct the expression of the contact relationship between the rolling element and the local defect edge at different stages of evolution. Investigating the influence of the local defect evolution on the vibration response of the rolling bearing.

Nomenclature

A	Long and half axis length of contact ellipse
B	Width of local defect
B_1	Width of centering surface of the cage
C	Total damping coefficient
c'	Radial clearance of the rolling bearing
c_1	Size of the cage guide clearance
c_r	Damping coefficient of oil film in the inlet region
D	Pitch diameter
d	Diameter of rolling element
E	Material elastic modulus
E'	Equivalent elastic modulus of material
e	Relative change amount of cage center
F_i	Oil film resistance
G	Dimensionless material parameter
H_o	Central oil film thickness
H_f	Additional displacement
$H_{\max}$	Maximum additional displacement
$h_{\min}$	Minimum oil film thickness
I	Inner race
i	Rolling element number
K	Contact stiffness
K_z	Total contact stiffness and damping
k	Ellipticity
k_i	Contact stiffness of rolling bearing with inner race
k_o	Contact stiffness of rolling bearing with outer race
k_r	Stiffness of oil film in the inlet region
k_y	Oil film stiffness of Hertz contact area
L	Length of the local defect
M	Mass of inner race and shaft
O	Outer race
O_{j_1}	Center of the race
O_{j_2}	Center of the race after deformation
Q	External load
Q'	Dimensionless load parameter
R_1	Radius of the centering surface of the cage
R'	Equivalent radius between rolling element and the race
R_i	Radius of inner race
U'	Dimensionless velocity parameter
u_x	Entrainment velocity
u_1	Entrainment Velocity of lubricating oil
v_M	Linear velocity of contact point M
v_N	Linear velocity of contact point N
z	Total number of the rolling element
β	Loading zone parameter for the ith rolling element
δ	Contact displacement
δ_i^*	Dimensionless contact deformation of inner race

δ_o^* Dimensionless contact deformation of outer race
ε Relative eccentricity of the cage center
η_0 Viscosity of oil film
θ_0 Initial contact angle
θ_i Contact angle between ith rolling element and rolling race
μ Friction coefficient
$\sum\rho_i$ Sum of curvature of the inner race
$\sum\rho_o$ Sum of curvature of the outer race
σ Poisson's ratio
Φq Defect angle
Φ_0 Initial position angle of ith rolling element to local defect
Φ_{di} Angular position for the ith rolling element with respect to X-axis
ω Oscillating frequency
ω_c Cage velocity
ω_s Shaft velocity
ω_m Revolution angular velocity of rolling element
ω_r Rotation angular velocity of rolling element

This work was supported by the National Natural Science Foundation of China (Grant No. 51775428), the Open Project of State Key Laboratory of Digital Manufacturing Equipment and Technology (Grant No. DMETKF2017014) and the Project of PhD Innovation Foundation of Xi'an University of Technology (Grant No. 310-252071701).

References

[1] A.B. Jones, Ball motion and sliding friction in ball bearings, J. Basic Eng. **81**, 1–12 (1959)
[2] P.K. Gupta, Advanced dynamics of rolling elements, Springer-Verlag, 1984
[3] A. Garad, V.J. Shinde, A theoretical model of deep groove ball bearing for predicting the effect of localized defects on vibration, Int. J. Mech. Eng. Technol. **8**, 760–769 (2017)
[4] L.K. Niu, H.R. Cao, X.Y. Xiong, Dynamic modeling and vibration response simulations of angular contact ball bearings with ball defects considering the three-dimensional motion of balls, Tribol. Int. **109**, 26–39 (2017)
[5] Y.C. Wang, Y.X. He, W. Weng, J.R. Liu, Frictional analysis of deep-groove ball bearings with varying circumference radial preloads, Adv. Mech. Eng. **9**, 1687814017703895 (2017)
[6] G.W. Yu, M. Su, W. Xia, R. Wu, Q. Wang, Vibration characteristics of deep groove ball bearing based on 4-DOF mathematical model, Proc. Eng. **174**, 808–814 (2017)
[7] A. Moshrefzadeh, A. Fasana, Planetary gearbox with localised bearings and gears faults: simulation and time/frequency analysis, Meccanica **52**, 3759–3779 (2017)
[8] I.M. Jamadar, D.P. Vakharia, A new damage diagnostic approach for deep groove ball bearings having localized surface defects in the raceways, J. Tribol. **9**, 1–10 (2017)
[9] R.K. Dewangan, S.P.S. Matharu, Evaluation of lubricant film thickness for ball bearings 6207 & 6307 with elliptical & circular contact area, Int. J. Eng. Technol. **9**, 208–216 (2017)
[10] L. Bizarre, F. Nonato, K.L. Cavalca, Formulation of five degrees of freedom ball bearing model accounting for the nonlinear stiffness and damping of elastohydrodynamic point contacts, Mech. Mach. Theory **124**, 179–196 (2018)
[11] R. Yang, Y.L. Jin, L. Hou, Y.S. Chen, Study for ball bearing outer race characteristic defect frequency based on nonlinear dynamics analysis, Nonlinear Dyn. **90**, 781–796 (2017)
[12] H. Wang, Q.K. Han, D.N. Zhou, Nonlinear dynamic modeling of rotor system supported by angular contact ball bearings, Mech. Syst. Signal Process. **85**, 16–40 (2017)
[13] C. Servais, J.L. Bozet, New computational method of the ball/race contacts transverse loads of high speed ball bearings without race control hypothesis, Tribol. Int. **113**, 206–215 (2017)
[14] T. Xu, G.H. Xu, Q. Zhang, C. Hua, H.H. Tan, S.C. Zhang, A.L. Luo, A preload analytical method for ball bearings utilising bearing skidding criterion, Tribol. Int. **67**, 44–50 (2013)
[15] N. Sawalhi, R.B. Randall, Simulating gear and bearing interactions in the presence of faults: Part I. The combined gear bearing dynamic model and the simulation of localised bearing faults, Mech. Syst. Signal Process. **22**, 1924–1951 (2008)
[16] Y.L. Wang, W.Z. Wang, Z.Q. Zhao, Effect of race conformities in angular contact ball bearing, Tribol. Int. **104**, 109–120 (2016)
[17] Y.L. Wang, W.Z. Wang, S.G. Zhang, Z.Q. Zhao, Investigation of skidding in angular contact ball bearings under high speed, Tribol. Int. **92**, 404–417 (2015)
[18] Q.K. Han, F.L. Chu, Nonlinear dynamic model for skidding behavior of angular contact ball bearings, J. Sound Vib. **354**, 219–235 (2015)
[19] L.K. Niu, H.R. Cao, Z.J. He, Y.M. Li, A systematic study of ball passing frequencies based on dynamic modeling of rolling ball bearings with localized surface defects, J. Sound Vib. **357**, 207–232 (2015)
[20] J. Liu, Z.F. Shi, Y.M. Shao, An analytical model to predict vibrations of a cylindrical roller bearing with a localized surface defect, Nonlinear Dyn. **89**, 2085–2102 (2017)
[21] B.J. Hamrock, D. Dowson, Isothermal elastohydrodynamic lubrication of point contacts: Part III—Fully flooded results, J. Tribol. **99**, 264–275 (1976)
[22] G.D. Hagiu, M.D. Gafitanu, Dynamic characteristics of high speed angular contact ball bearings, Wear **211**, 22–29 (1997)
[23] Case Western Reserve University Bearing Data Center Website http://csegroups.case.edu/bearingdatacenter/home

Cite this article as: J. Kang, Y. Lu, Y. Zhang, C. Liu, S. Li, N. Müller, Investigation on the skidding dynamic response of rolling bearing with local defect under elastohydrodynamic lubrication, Mechanics & Industry **20**, 615 (2019)